Pathogenic mutations and T cell involvement in progression stages of cutaneous melanoma

Optimizing the quantification of molecular genetic changes
by digital droplet PCR technology

Final thesis

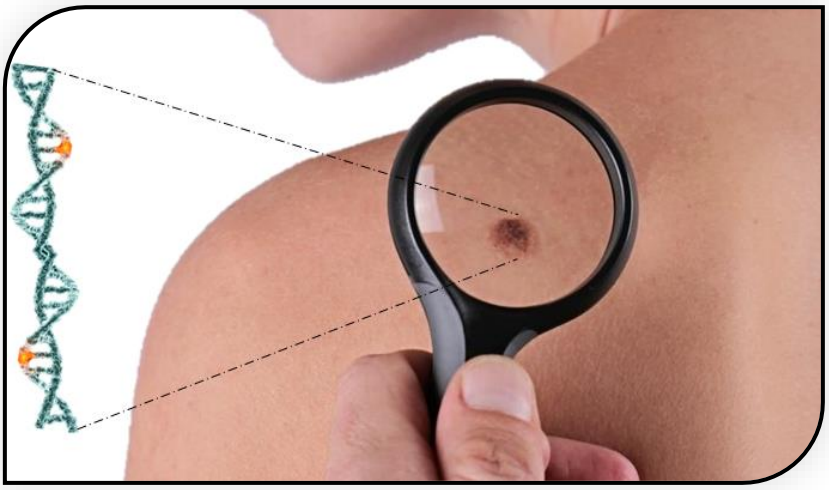

Johnny Aarnoutse
Chemistry program, Academy for Technology & Innovation,
HZ University of Applied Sciences

Final thesis submitted for the degree of
Bachelor of Science

Leiden, January 6st, 2018

Pathogenic mutations and T cell involvement in progression stages of cutaneous melanoma

Optimizing the quantification of molecular genetic changes by digital droplet PCR technology

Johnny Aarnoutse
Final thesis
HZ University of Applied Sciences
Major Life Sciences, Chemistry
Leiden, January 6st, 2018

In-company mentor:
N.A. (Nelleke) Gruis, Ph.D.

Work placement lecturer:
K.F. (Kas) Wannee, M.Sc.

Abbreviations

BRAF	Proto-oncogene *BRAF*
C	Constant segment
Cq	Cycles of quantification
D	Diversity region
ddPCR	Droplet digital Polymerase Chain Reaction
ERK	Extracellular Signal-regulated Kinase
FAM	Fluorescein amidite dye
FDA	Food and Drug Administration
FFPE	Formalin-fixed paraffin-embedded
HEX	Hexachloro-fluorescein dye
J	Joining segment
LNA	Locked nuclei acid
MAPK	Mitogen-activated protein kinase
NA	Nucleic acid
MEK	Mitogen-activated protein kinase/ Extracellular Signal-regulated Kinase
PCR	Polymerase Chain Reaction
qPCR	Real-time polymerase chain reaction
RPL13	60S ribosomal protein L13
RPS11	ribosomal protein S11
TCR	T cell receptor
TRD	T cell receptor delta
TTC5	Tetratricopeptide repeat domain 5
UV	Ultraviolet
V	Variable segment

Abstract

Cutaneous melanoma is a type of skin cancer that develops from benign melanocytes to one of the most aggressive types of skin tumors in human. In cutaneous melanoma progression, the metastasis phase is the most challenging phase to treat. To enable earlier treatment options, a better understanding of the development of this disease is essential. The current knowledge proposes that the stepwise development of melanoma is driven by succession of driver mutations. A common driver in the early stages of melanoma is the V600E mutation in the *BRAF* oncogene. Though, progression from a benign stage to a malignant lesion is not always the case. This might be the result of alternative exon splicing of the *BRAF* gene. Once the melanoma progresses, an increasing amount of T cells can be observed. Despite the fact that *BRAF* V600E mutations, splice variants and T cells do play a role in melanoma progression, exact quantitative information is still poorly investigated. In this project, the main goal was to optimize the quantification of molecular genetic changes by digital droplet PCR technology in different progression stages of cutaneous melanoma using formalin-fixed paraffin-embedded material derived from dysplastic nevi and melanoma lesions. The central question in this project was: In which quantities are BRAF splice variants and T cells present in the different progression stages of cutaneous melanoma and is the *BRAF* V600E mutation connected to the occurrence of splice variants? The results showed that spice variants were present in the *BRAF* transcripts. However, the exact genomic region where splice variants occurred and the exact connection with the *BRAF* V600E mutation could not be confirmed. Regarding to T cell quantification, it can be concluded that melanoma contained more T cells than dysplastic nevi. Further research on these subjects is recommended, starting with further optimization of the experiments.

Table of contents

1. Introduction

Cutaneous melanoma is a type of skin cancer that develops from melanocytes to one of the most aggressive types of skin tumors in human (Bandarchi, Ma, Navab, Seth, & Rasty, 2010). As the disease advances, tumor cells invade into the bloodstream and/or lymph vessels, causing metastasis in other organs of the body leading eventually to death (Martin TA, 2013). The prevalence of melanoma has been increasing over the past decades due to increased sun exposure. At this moment, 132.000 melanoma skin cancers occur worldwide each year ("World Health Organization," 2017).

The progression of cutaneous melanoma is driven by succession and accumulation of driver mutations (Bastian, 2014; Shain *et al*., 2015). One of these drivers is the V600E mutation in the *BRAF* oncogene. BRAF is a regulator of the RAS/MAPK signaling pathway. This signaling pathway is essential for several cellular processes such as proliferation, differentiation, apoptosis and survival (Shain *et al*., 2015; Spagnolo, Ghiorzo, & Queirolo, 2014). Different mutations of the *BRAF* gene have been reported that hyper activate the RAS/MAPK pathway. An increase in protein expression or activity can disturb the RAS/MAPK signaling pathway, which can lead to uncontrolled cell division (Hussain *et al*., 2015).

Different progression stages can be distinguished during the stepwise transformation from benign melanocytes to metastatic melanoma (Bastian, 2014). The V600E *BRAF* mutation is already observed in benign nevi and the early progression stage of melanoma: the atypical nevus (Shain *et al*., 2015). In 60% of primary melanomas, the V600E mutation has been detected (Bruno *et al*., 2017). However, it is not completely understood in which quantities the *BRAF* V600E mutation occurs in each progression stage although this information may be important to make a clear difference between benign and malignant stages.

Nevertheless, progression from a benign stage to a malignant lesion is not always the case. This might be the result of alternative exon splicing of the *BRAF* gene. During this process, particular exons can be excluded from the final processed messenger RNA which can lead to altered biological functions of proteins (Black, 2003). Parallel with molecular development, immunogenic processes play a role as well. T cell infiltration of tumors is a common phenomenon. However, melanoma cells have the capacity to suppress the immune microenvironment to promote constant growth (Chen *et al*., 2017). However, the relation between T cell infiltration and progression stages in cutaneous melanoma is not exactly understood.

In this project, the main goal was to optimize the quantification of molecular genetic changes by digital droplet PCR (ddPCR) technology in different progression stages of cutaneous melanoma using formalin- fixed paraffin-embedded (FFPE) material. Eventually, the optimized techniques might enable absolute quantification of molecular genetic changes. A better discrimination between benign and malignant melanoma upon which better patient treatment might be possible. Our main research question therefore is: In which quantities are *BRAF* splice variants and T cells present in the different progression stages of cutaneous melanoma and is the *BRAF* V600E mutation connected to the occurrence of splice variants?

2. Theoretical framework

2.1 Cutaneous melanoma

Cutaneous melanoma is a life-threatening type of skin cancer that develops in the melanocytes – the pigment-containing cells colonized in the basal layer of the epidermis (Bandarchi *et al*., 2010). The disease can be characterized by complex interactions on molecular level which leads to a stepwise transformation from melanocytes to metastatic melanoma (Bastian, 2014). Melanomas are commonly of cutaneous origin, nevertheless, they may rarely arise in the mouth, intestines, or even in the eyes (Mihajlovic, Vlajkovic, Jovanovic, & Stefanovic, 2012).

2.1.1 Progression stages in cutaneous melanoma

Neoplasm of melanocytes in the skin results in the formation of a benign nevus. The development of cutaneous melanoma progresses when the benign nevus transforms into an intermediate nevus (atypical nevus or dysplastic nevus). Subsequently, the intermediate nevus might grow out into a primary melanoma. Eventually, metastatic melanoma progresses when the primary tumor cells gain the capacity to invade, migrate and affect other organs in the body such as the lungs, liver and brain (Figure 1) (Elder, 2016), (Miller & Mihm, 2006).

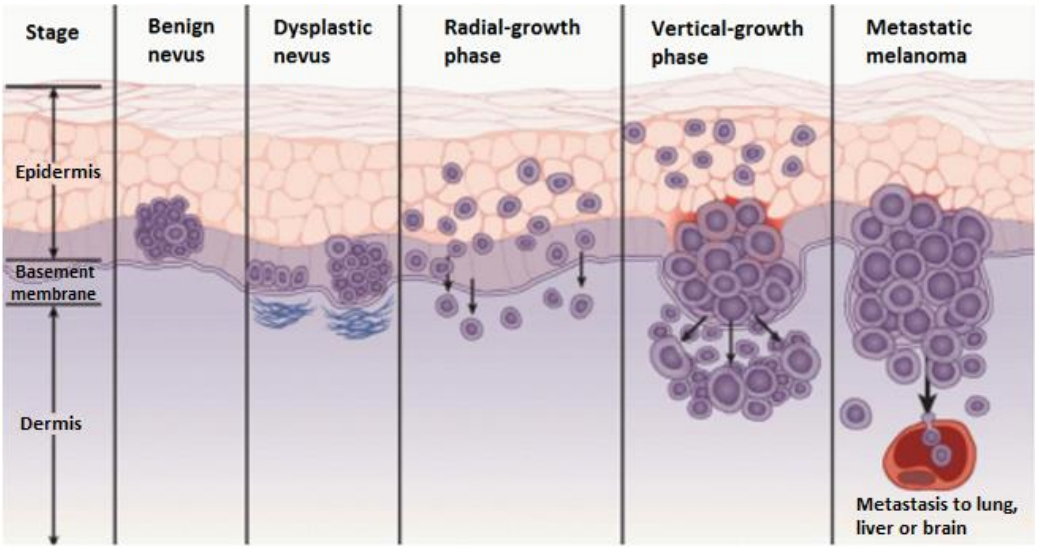

Figure 1. Biological events in the progression of cutaneous melanoma. (Miller & Mihm, 2006).

The survival rates of cutaneous melanoma become worse when the disease advances. Clinically, cutaneous melanoma is divided in four established stages (Balch *et al*., 2009; Balch *et al*., 2004) (Figure 2). Patients diagnosed with cutaneous melanoma at stage I, have a five-year survival rate of more than 90%. When diagnosed at stage IV, the five-year survival rate decreases to about 15% to 20%. Therefore, understanding the development of cutaneous melanoma at an early stage is critical for early diagnosis and treatment options ("Key Statistics for Melanoma Skin Cancer," 2017).

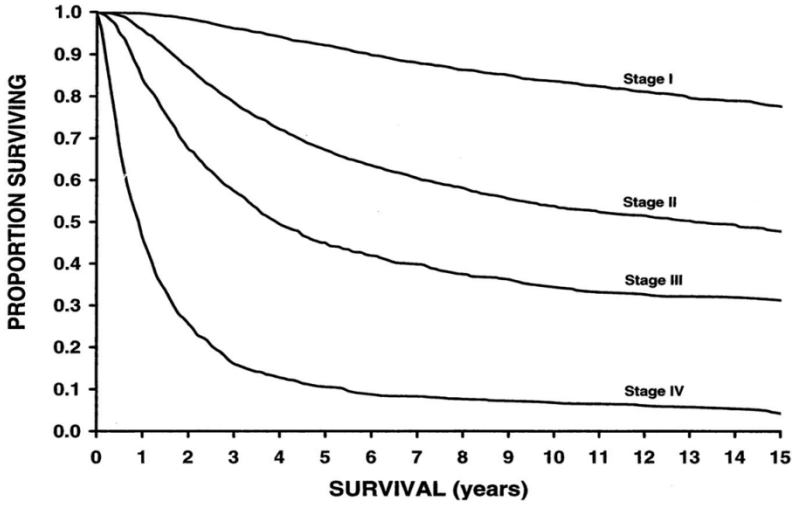

Figure 2. Stage 0 non-invasive melanomas are located only in the outer layer of the skin while stage I melanomas have already invaded. Though, these tumors are small and grow at a slow mitotic rate. Localized stage II tumors (intermediate melanomas) are larger and their mitotic rate increases. More advanced melanomas (Stages III and IV) have metastasized which results in tumor growth in other parts of the body resulting in a decrease in survival rate (Balch *et al*., 2004).

2.1.2 Driver mutations in melanoma progression

As for many other cancers, it has been suggested that the progression to a malignant melanoma is driven by succession and accumulation of driver mutations (Bastian, 2014; Shain *et al*., 2015). Previous whole exome and genome sequencing studies have identified many mutated genes in melanoma (Hodis *et al*., 2012; Krauthammer *et al*., 2012). However, these mutations are not all necessarily drivers of cutaneous melanoma progression. Based on the functional effects of the mutations, they can be identified as driver mutations.

One of the previously identified driver mutations is the *BRAF* V600E mutation. In this mutation, valine is substituted by glutamic acid at codon 600. The genetic alteration of *BRAF* has shown that it is able to disturb the cell growth and survival via affecting the mitogen-activated protein kinase (MAPK) signaling pathway (Bastian, 2014; McCain, 2013; Spagnolo *et al*., 2014). In 60% of primary melanomas, the V600E mutation has been detected (Bruno *et al*., 2017). The quantity in which the *BRAF* V600E mutation occurs within the different progression stages is still not completely clarified.

2.2 *BRAF* and the MAPK signaling pathway

BRAF is an oncogene that encodes the protein B-RAF. This gene is part of the RAF family and shows serine/threonine kinase activity ("National Center for Biotechnology Information," 2017). BRAF plays a role in the regulation of the MAPK signaling pathway (Figure 3).

More specifically, B-RAF facilitates phosphorylation of a second protein kinase in the MAPK signaling cascade. The starting point of this signaling cascade is the binding of a ligand to the receptor tyrosine kinase. The ligand, often a growth factor, is able to activate the receptor's activity. Activation of the receptor triggers the downstream phosphorylation and activation of the RAS, RAF, MEK1/2 and ERK1/2 proteins. Eventually, ERK (MAPK) activation lead to activation of gene transcription that regulates cell growth, proliferation and survival (Volinsky & Kholodenko, 2013).

These processes can start to be at risk once *BRAF* gets mutated. Mutated *BRAF* activates the RAS/MAPK pathway. Additionally, an increase in protein expression or activity can in turn result in uncontrolled cell division (Hussain *et al*., 2015). Based on these oncogenic characteristics, several drug design campaigns have yielded potent BRAF inhibitors. The therapeutic agents vemurafenib and dabrafenib were approved by the US Food and Drug Administration (FDA) for *BRAF*-mutated melanoma treatment (Holderfield, Deuker, McCormick, & McMahon, 2014; McCain, 2013).

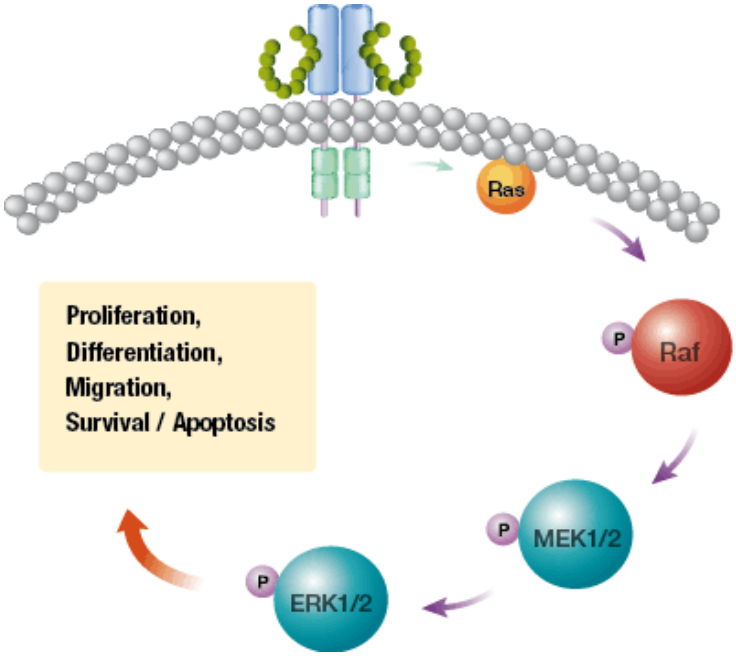

Figure 3. Representation of the MAPK signaling pathway. Binding of a ligand to the receptor tyrosine kinase activates the receptor's activity. Activation of the receptor triggers the downstream phosphorylation and activation of the RAS, RAF, MEK1/2 and ERK1/2 proteins which results in gene transcription. The resulting transcript regulates cell growth, proliferation, and survival ("National Cancer Institute," 2017).

2.3 Alternative splicing of *BRAF*

The therapeutic agents, described in 2.2, improve the overall survival of patients having *BRAF*-mutant melanoma (Chapman *et al*., 2011). In spite of this activity, multiple acquired resistance mechanisms in melanoma patients have been described (Rizos *et al*., 2014). Yet, the frequency of these mechanisms and correlation with clinical outcome to BRAF inhibitor therapy is poorly understood.

Though, previous studies have shown that alternative exon splicing of the oncogenic *BRAF* transcript is the most common driver of acquired resistance to vemurafenib and dabrafenib as a consequence of reduced affinity to these therapeutic agents (Poulikakos *et al*., 2011; Rizos *et al*., 2014). The resistance mechanism is evident in approximately 30% of resistant melanomas (Salton *et al*., 2015; Spagnolo *et al*., 2014). However, it is not exactly known when alternative splice variants play a role in progression of cutaneous melanoma.

Alternative splicing can be characterized as a controlled process during gene expression. During this process, particular exons can be excluded from the final processed messenger RNA (mRNA) (Black, 2003). Consequently, the proteins translated from alternatively spliced mRNAs will contain differences in their amino acid sequences which can result in different biological functions.

A previous study has recently identified a *BRAF* splice variant in a single vemurafenib resistant melanoma cell line (Salton *et al*., 2015). The *BRAF* transcript was lacking exons 4-8, which contain critical domains for the activation of RAF. As a result of the deletion of exons 4-8, an impaired feedback mechanism can be expected. Therefore, it is important to elucidate when alternative splicing plays a role in progression of cutaneous melanoma and in which ratio.

2.4 T cell involvement in cutaneous melanoma

Cutaneous melanoma can be considered as an immunogenic tumor type. The tumor often encompasses considerable amounts of both innate as well as adaptive immune cells that might reflect a reaction against the tumor (Gajewski, Meng, & Harlin, 2006; Houghton, Gold, & Blachere, 2001). It is known that T cell infiltration of tumors is a common phenomenon. T cell infiltration has clinical consequences. Previous studies have shown that that migration of T cells in the direction to tumors and the extent of infiltration have been correlated positively with clinical prognosis and negatively to tumor growth which leads to higher survival rates (Fridman *et al*., 2011; Talmadge, 2011).

How T cell infiltration is precisely related to the progression stages in cutaneous melanoma is not exactly known. Quantification of infiltrating T cells in progression stages might give more insight in the underlying mechanism. These findings can be valuable with respect to (individualized) therapies, diagnostics and prognostics.

2.5 T cell receptor rearrangements

To determine the proportion of T cells in the different progression stages of cutaneous melanoma, ddPCR was used to measure loss of T cell receptor (TCR) loci on germline DNA. The exact method to measure this loss can be found in chapter 3. In the next section, the theoretical background of (TCR) gene rearrangements is further elaborated which helps to understand the method used for quantifying T cells accurately.

Mature T cells differ genetically from other cell types as a result of TCR gene rearrangements. Gene rearrangement is a unique process of genetic recombination that occurs only in developing lymphocytes, including T cells (Charles A Janeway, 2001; Li *et al*., 2016). Four gene complexes, called *TRD*, *TRG*, *TRB* and *TRA*, are responsible for the variety of expressed TCRs. These complexes rearrange sequentially in a ordered manner, where after a functional recombined TCR sequence is acquired (Dik *et al*., 2005; Zoutman *et al*., 2017). In this project, the focus was on gene complex *TRD*.

The *TRD* gene complex, located on chromosomal position 14q11.2, is composed of constant (C) and variable (V) regions which are assembled together during the development by rearrangement in the thymus (Figure 4). The *TRD* chains are assembled from V, diversity (D), and joining (J) segments. All of the non-consecutive V, D, and J segments are subjected to rearrangement during T cell development to form eventually complete V domain exons, which makes sure that antigens can be recognized. During TCR gene rearrangement and several nucleotide insertions and deletions, the V, D, and J segments are brought together into continuous V–D–J coding blocks which account for the diversity and specificity necessary for recognizing the huge variety of non-self -antigens (Hodges, Krishna, Pickard, & Smith, 2003).

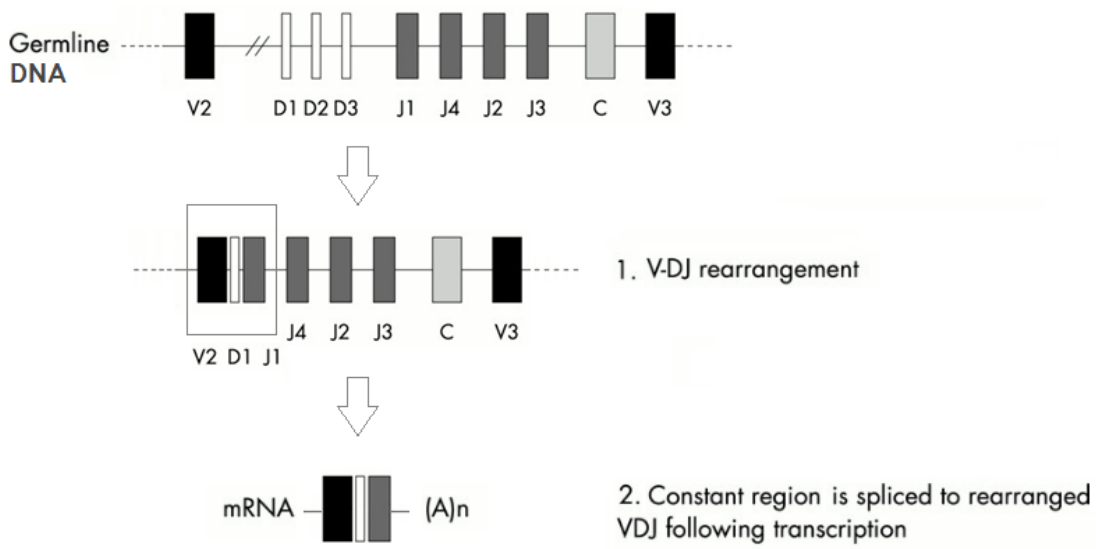

Figure 4. Germline organization of the *TRD* locus situated on chromosome 14. The type of gene segments are indicated by shaded boxes: V, variable (black); D, diversity (white); J, joining (dark grey); C, constant (light grey). The recombination of the *TRD* locus is a process of two steps in which a D segment first recombines with a J segment. Secondly, the DJ block recombines with a V segment. Then, the rearranged VDJ segment is spliced post transcriptionally in order to form a functional T cell receptor (Hodges *et al*., 2003).

2.6 Research outline

To optimize the detection and quantification of molecular genetic changes in different progression stages of cutaneous melanoma, ***BRAF* splice variants** and **tumor-infiltrating T cells** were investigated by using the real-time polymerase chain reaction (qPCR) and/ or ddPCR. Detection of *BRAF* splice variants was performed by using qPCR. qPCR monitored RNA levels of splice variants by using different primer sets. Quantification of splice variants and T cells was performed with ddPCR.

The ddPCR technique was able to measure absolute quantities by counting nucleic acid molecules that are encapsulated in water-in-oil emulsion droplets. A sample was fractionated into 20,000 droplets, and PCR amplification of the template molecules occurred in each individual droplet. The massive sample partitioning which was combined with Poisson statistical data analysis can be considered as a key aspect of the ddPCR technique.

Chapter 3 describes the steps taken to prepare the samples properly before starting experiments. In addition, it puts forward the methods used to optimize the detection and quantification of *BRAF* splice variants and T cells more detailed.

3. Materials and methods

3.1 Isolation of genomic material and sample preparation

Isolation and cDNA synthesis of RNA from conjunctival melanoma cell lines

For optimization purposes, conjunctival melanoma cell lines CRMM.1, CRMM.2 (Nareyeck, Wuestemeyer, von der Haar, & Anastassiou, 2005) and CM2005.1 (Keijser, Maat, Missotten, & de Keizer, 2007) were used. The cell lines CRMM.1 and CM2005.1 were known to harbor the *BRAF* V600E mutation, while CRMM.2 was known to have a *BRAF* wild type.

RNA of all conjunctival melanoma cell lines was isolated using the RNeasy Mini Kit (Qiagen, Hilden, Germany). After RNA isolation, the concentration of RNA was measured with a spectrophotometer (NanoDrop Technologies, San Francisco, USA). For quality control, the 260/280 nm ratio was determined. In addition, RNA integrity was determined using the Experion RNA Analysis Kit (Bio-Rad, Mississauga, Canada).

Isolated RNA was subsequently reversed transcribed into cDNA using the iScript^{TM} cDNA Synthesis Kit (Bio-Rad, Mississauga, Canada). A RNA/H_2O mixture with a maximal input of 500 ng/7.5 µL was mixed with a master mix, consisting of iScript reaction mix, provided by the kit, and reverse transcriptase. The prepared samples were subsequently subjected to the PCR machine (Bio-Rad, Mississauga, Canada). Finally, synthesized cDNA samples were diluted five times with TE-buffer (10 mM Tris, 1 mM EDTA) to make the samples ready for qPCR where after the samples were stored in the freezer at -20 °C.

Isolation of nucleic acid from formalin-fixed paraffin-embedded material

Formalin-fixed paraffin-embedded (FFPE) tissue samples of different melanoma progression stages were used to perform the actual experiments. These samples were obtained from the LUMC pathology archives. Confirmation of clinical diagnosis of FFPE samples is represented in table S5 in appendix 3.

Nucleic acid (NA) was isolated from all FFPE tissue samples. Ten sections of 10 µm were cut by a microtome and subsequently used to extract NA with the kPCR Sample Prep robot (VERSANT, Siemens Healthineers, Erlangen, Germany) at the pathology department of the LUMC. Extraction was performed using Versant Tissue Preparation Reagents (Siemens).

3.2 Optimization of *BRAF* splice variant and *BRAF* driver mutation experiments

Sample selection

cDNA from CRMM1, CRMM2 and CM2005.1 conjunctival melanoma cell lines was used to optimize the detection and quantification of the *BRAF* V600E mutation and the splice variants of *BRAF*. cDNA from monolayer cultured keratinocytes and fibroblasts was used as control. H_2O was used as negative control for PCR contamination.

Design of primers and probes

Multiple PCR primers were designed to span exons 14 and 15. Depending on the primers, the *BRAF* V600E mutation located on exon 15 (when present), was spanned as well. In addition, PCR primers were designed to span exons 8 and 9 (Sigma-Aldrich, St. Louis, Missouri, United States). Moreover, fluorescein amidite- and hexachloro-fluorescein-labelled probes (FAM -and HEX-labelled probes) (Sigma-Aldrich) were designed for ddPCR experiments to target and quantify the genomic regions of interest accurately. Primer and probe information is represented in table S1 and S2 respectively in appendix 1.

Testing primers with qPCR

Splice variants of *BRAF* were investigated with qPCR. A master mix, which contained synthesized cDNA, SYBR Green, forward primer, reverse primer and H_2O was prepared before performing qPCR. The mixtures were transferred into a 384-well plate and subsequently subjected to the PCR machine (Bio-Rad). Cycle parameters were as follows: 3 minutes at 95 °C; denaturation for 10 seconds at 96 °C and annealing and extension for 30 seconds at 60 °C for 39 cycles and subsequently 10 minutes at 95 °C. Finally, data evaluation was performed using Bio-Rad CFX Manager version 3 (Bio-Rad, Mississauga, Canada). The most stable reference genes were determined by the geNorm application (Vandesompele *et al*., 2002).

Testing primers and probes with ddPCR

Splice variant detection by ddPCR was performed using ddPCR Supermix for probes, forward primers, reverse primers and probes (Bio-Rad Laboratories, Hercules, CA) in 22 µL with 10-25 ng cDNA. Each sample was converted to an emulsion of 20.000 droplets using an automated droplet generator and DG8 cartridges (Bio-Rad). Emulsified samples were subsequently transferred to a 96-well PCR plate for amplification in a T100 Thermal Cycler (Bio-Rad). Cycle parameters were as follows: 10 minutes at 95 °C; denaturation for 30 seconds at 94 °C and annealing and extension for 1 minute at 60 °C for 39 cycles; subsequently 10 minutes at 98 °C; and infinite cooling at 12 °C. The ramp rate for all cycles was 2 °C /second. Cycled droplets were stored at 4 °C to 12 °C until reading.

After amplification, the plate was transferred to a QX200 Droplet Reader (Bio-Rad) which sips droplets from each well and streams them past a two-color FAM/HEX fluorescence detector. Positive droplets (containing amplified target DNA) and negative droplets (do not contain amplified target DNA) were used to divide the droplet population into four separate groups: HEX-/FAM- which contained no target, HEX+/FAM- which contained only *BRAF* 14-15, HEX-/FAM+ which contained only *BRAF* 8-9 and HEX+/FAM+ that contained both *BRAF* 14-15 and *BRAF* 8-9. Quantified droplets corrected by Poisson's law resulted in the initial target concentrations and were analyzed and normalized using QuantaSoft software version 1.7.4 (Bio-Rad).

3.2.1 Optimized detection of *BRAF* splice variants

By using multiple combinations of primers (and probes), splice variants can be observed by qPCR and ddPCR by applying the methods described in paragraph 3.2. qPCR amplification curves and melt peak curves might respectively show different Cq values and multiple melt peaks as a consequence of alternative splicing. ddPCR might show different amounts of events per droplet and variable initial target concentrations. Figure 5 shows schematically where primers anneal along exon 8-9 and exon 14-15 of the *BRAF* gene.

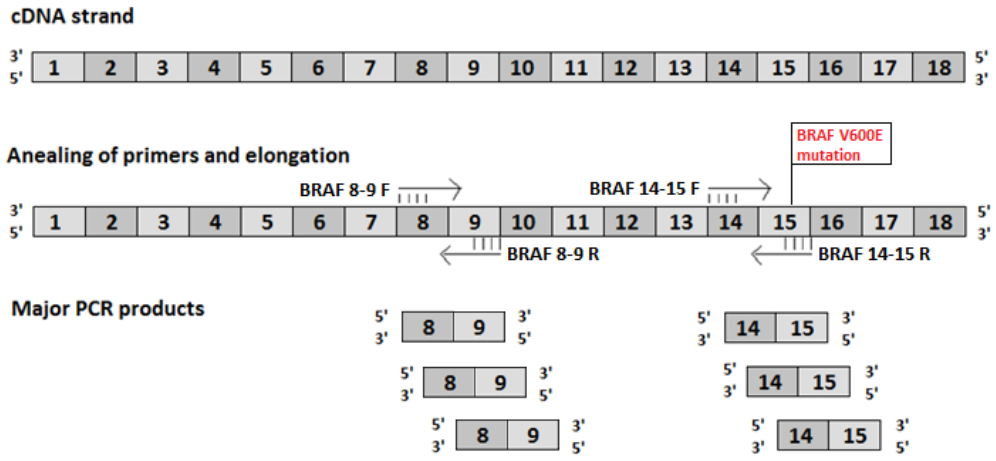

Figure 5. The *BRAF* gene consists of 18 exons. A combination of *BRAF* 8-9 and *BRAF* 14-15 primer sets was used to amplify exon 8-9 and exon 14-15 respectively.

3.3 Optimized quantification of tumor-infiltrating T cells

The next section describes the exact method used to quantify T cells by measuring loss of germline *TRD* genomic locus by means of ddPCR. The method is based on measuring a locus which is frequently deleted in TCR genes of T cells as a consequence of rearrangements as earlier described in chapter 2. This can give insight in the contribution of T cells in between non-T cells, in which no rearrangements occur (Figure 6).

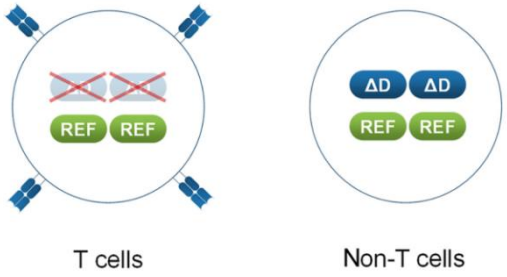

Figure 6. As a result of genomic TCR recombination in T cells, T cells and non-T cells are genetically different. In contrast to non-T cells, T cells are lacking TCR locus (ΔD) biallelically (Zoutman *et al*., 2017).

As most suitable target, the intergenic sequence Dδ2-Dδ3 (also called ΔD) was used (Figure 7). Since rearrangements occur at both alleles of T cells, all these cells are virtually lacking ΔD (Dik *et al*., 2005). T cell quantity can be determined accurately by measuring loss of this specific TCR locus and by normalizing against a copy number stable reference gene, (Zoutman *et al*., 2017).

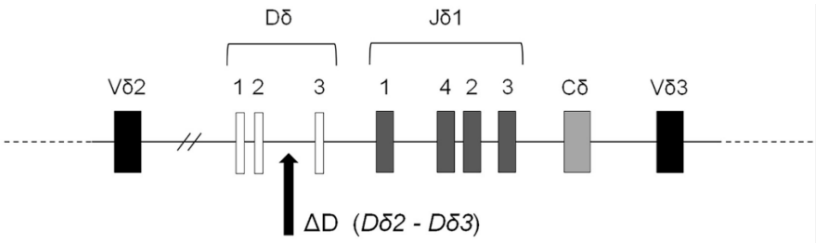

Figure 7. Schematic representation of a part of the *TRD* gene complex. ΔD specifies the noncoding sequence, located between the Dδ2 and Dδ3 genes and is deleted biallelically by TCR rearrangements during T cell development (Zoutman *et al*., 2017).

For accurate T cell quantification, primers and FAM- or HEX-labelled probes were used. Probes directed against target locus ΔD, were labelled with FAM, while probes directed against the reference gene (*TTC5*) were labelled with HEX (Table 1).

Table 1. Primer and probe information

Gene	Genomic feature	Forward primer (900 nmol·L^{-1})	Reverse primer (900 nmol·L^{-1})	Probe (250 nmol·L^{-1})	Label
TRD	Dδ2-Dδ3 (ΔD)	5'-GCTGGCTGTAAT-GGGAATGT-3'	5'-TAATGGCTTGATAA-AGATAAGTGATCAT-3'	5'-TGTGAAGATGTCT-GTAGCCATCTTAT-3'	FAM
TTC5	Exon 10	-	-	-	HEX

ddPCR for T cell quantification was performed using NA originating from FFPE tissue samples. Samples were diluted 10 times and 100 times with H_2O to prevent possible degradation of droplets by the buffer in which isolated NA was solubilized. Undiluted samples were evaluated as well. A reaction mixture of 20 µL was used which contained ddPCR Supermix for probes (Bio-Rad Laboratories, Hercules, CA). Each sample was subsequently converted to an emulsion of 20.000 droplets using an automated droplet generator and DG8 cartridges (Bio-Rad).

Afterwards, the droplet emulsion was transferred to a 96-well PCR plate for amplification in a T100 Thermal Cycler (Bio-Rad). Cycle parameters were as follows: denaturation for 30 seconds at 94°C and annealing and extension for 1 minute at 60°C for 40 cycles; and infinite cooling at 12°C. The ramp rate for all cycles was 2°C/second.

Finally, droplets were analyzed and normalized using QuantaSoft software version 1.7.4 (Bio-Rad). To calculate normalized haploid copy numbers for ΔD, *TTC5* was used as a genomic copy number stable reference (REF) gene. The T cell fractions were calculated by subtracting the ratio between ΔD and *TTC5* from 1. The calculation was performed according to the formula represented below:

$$\textbf{T cell fraction} = 1 - \frac{\Delta D}{REF} \times 100\%$$

4. Results

4.1 Optimization of *BRAF* splice variant experiments

Testing 'BRAF 8-9*', 'BRAF* 14-15*' and BRAF qp 14-15 primers with qPCR*

The relative gene expression of target exons (*BRAF* 8-9 and *BRAF* 14-15) was measured by qPCR in cDNA of conjunctival melanoma cell lines using *BRAF* 8-9 and *BRAF* 14-15 forward and reverse primers. Moreover, a non-BRAF V600(E) overlapping qp 14-15 reverse primer was used. Relative gene expressions were normalized with *RPS11* and *RPL13* as they were determined by the software to be the most stable reference genes.

CM2005.1 showed the highest *BRAF* 8-9 expression whereas CRMM1 and CRMM2 showed a notable low expression (Figure 8A). Approximately the same relative normalized *BRAF* 14-15 expressions were found in all cell lines when using *BRAF* 14-15 forward and reverse primers (Figure 8B). When using a *BRAF* 14-15 forward primer in combination with a qp 14-15 reverse primer, CM2005.1 showed the highest *BRAF* 14-15 expression whereas CRMM1 and CRMM2 showed a notable low expression (Figure 8c).

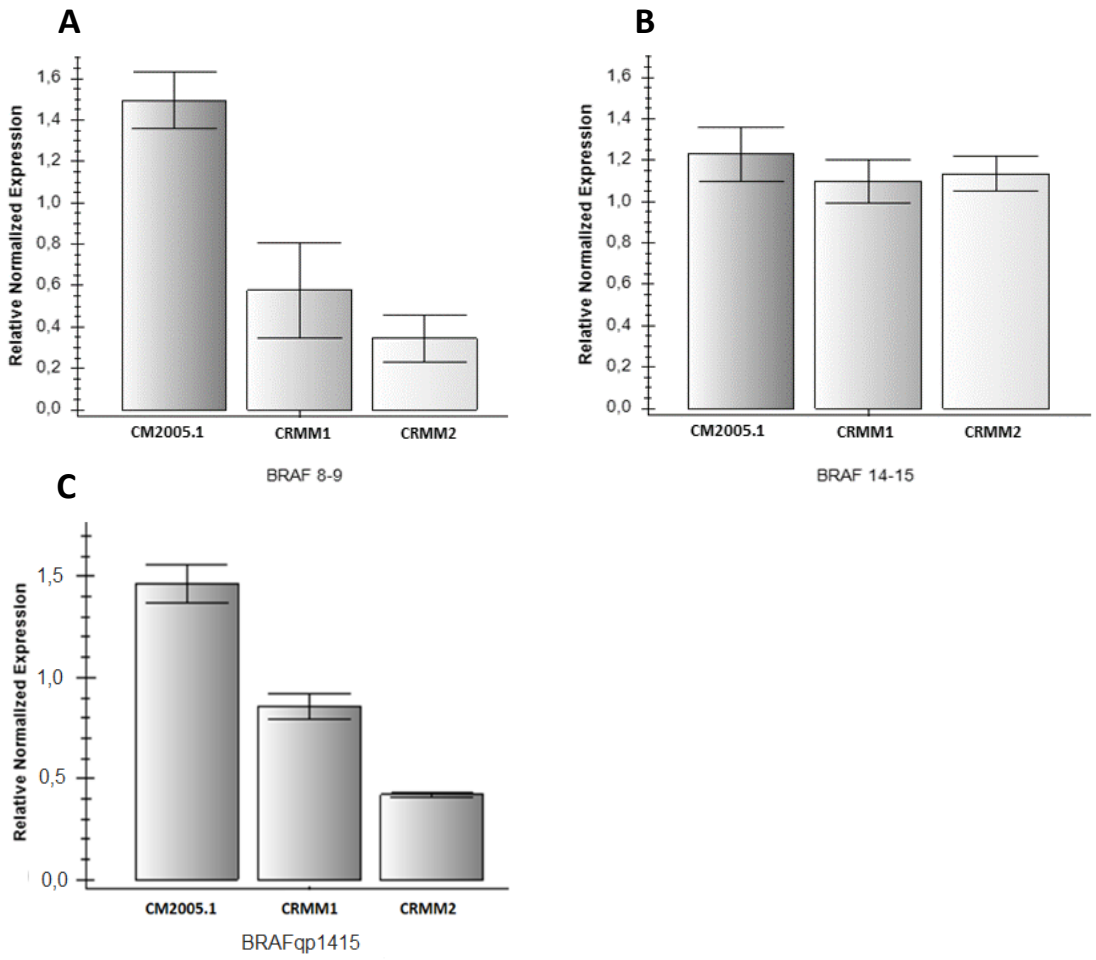

Figure 8. Relative normalized gene expression of *BRAF* 8-9 (A) and *BRAF* 14-15 (B and C) in cDNA of conjunctival melanoma cell lines measured with qPCR. Data were normalized using *RPS11* and *RPL13* as most stable reference genes.

Amplification of target exons measured at real-time showed that samples needed less than 30 cycles to reach the threshold which was set on 200 Relative Fluorescence Units (RFU) (Figure 9). Amplification of *BRAF* 8-9 showed in CM2005.1 a cq value of 25.24 while CRMM.1 and CRMM.2, showed an average cq value of 26.17 and 26.99 respectively. Approximately the same cq values, lying around 28 cycles, were found in all conjunctiva melanoma cell lines when *BRAF* 14-15 was amplified. Additional corresponding raw data is shown in table S3 in appendix 2.

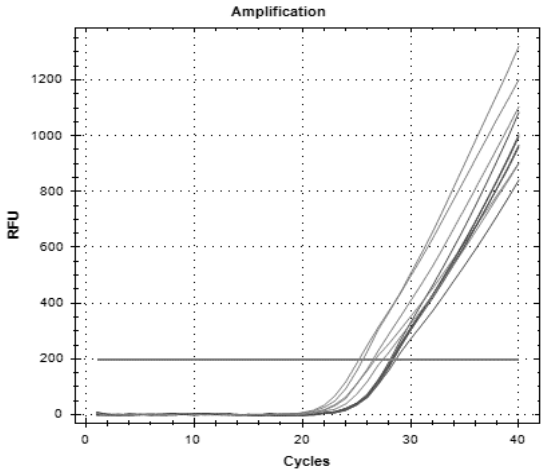

Figure 9. qPCR amplification chart demonstrates the amount of amplification product which is expressed in Relative Fluorescence Units as function of the amount of circles.

The melt peak was measured to determine whether dissociation-characteristics of amplified target cDNA occurred during heating (Figure 10). The double strand dissociated before 80°C for each cDNA sample, which eventually lead to an increased absorbance intensity (Figure 10).

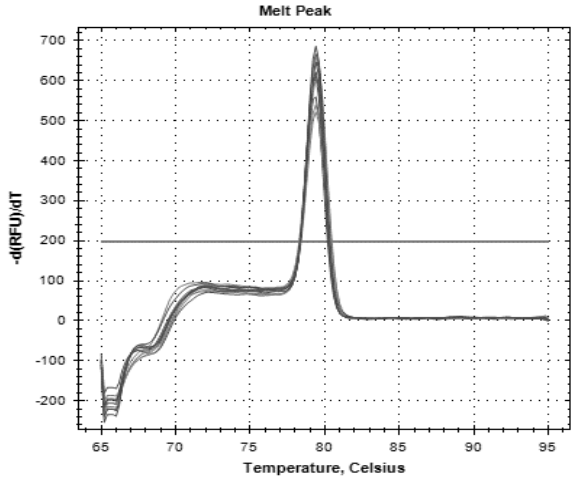

Figure 10. The melt peak (B) shows the relation between the first derivative of RFU and the temperature and indicates the melt peak.

Testing 'BRAF 8-9*' and 'BRAF* 14-15*' primers with ddPCR*

ddPCR demonstrates both *BRAF* 8-9 (Figure 11A) and *BRAF* 14-15 (Figure 11B) positive droplets in all samples, including keratinocytes and fibroblasts samples which were used as controls. However, CRMM1 and CM2005.1 positive droplets containing *BRAF* 14-15 did not show a clear separation with negative droplets. They demonstrated abundant intermediate droplets ('rain') that fall between the major positive and negative bands. Droplets were divided in four droplet populations: HEX-/FAM- droplets which contained no target (black), HEX+/FAM- droplets which contained only *BRAF* 14-15 (green), HEX-/FAM+ which contained only *BRAF* 8-9 (blue) and HEX+/FAM+ which contained both targets (orange) (Figure 11C).

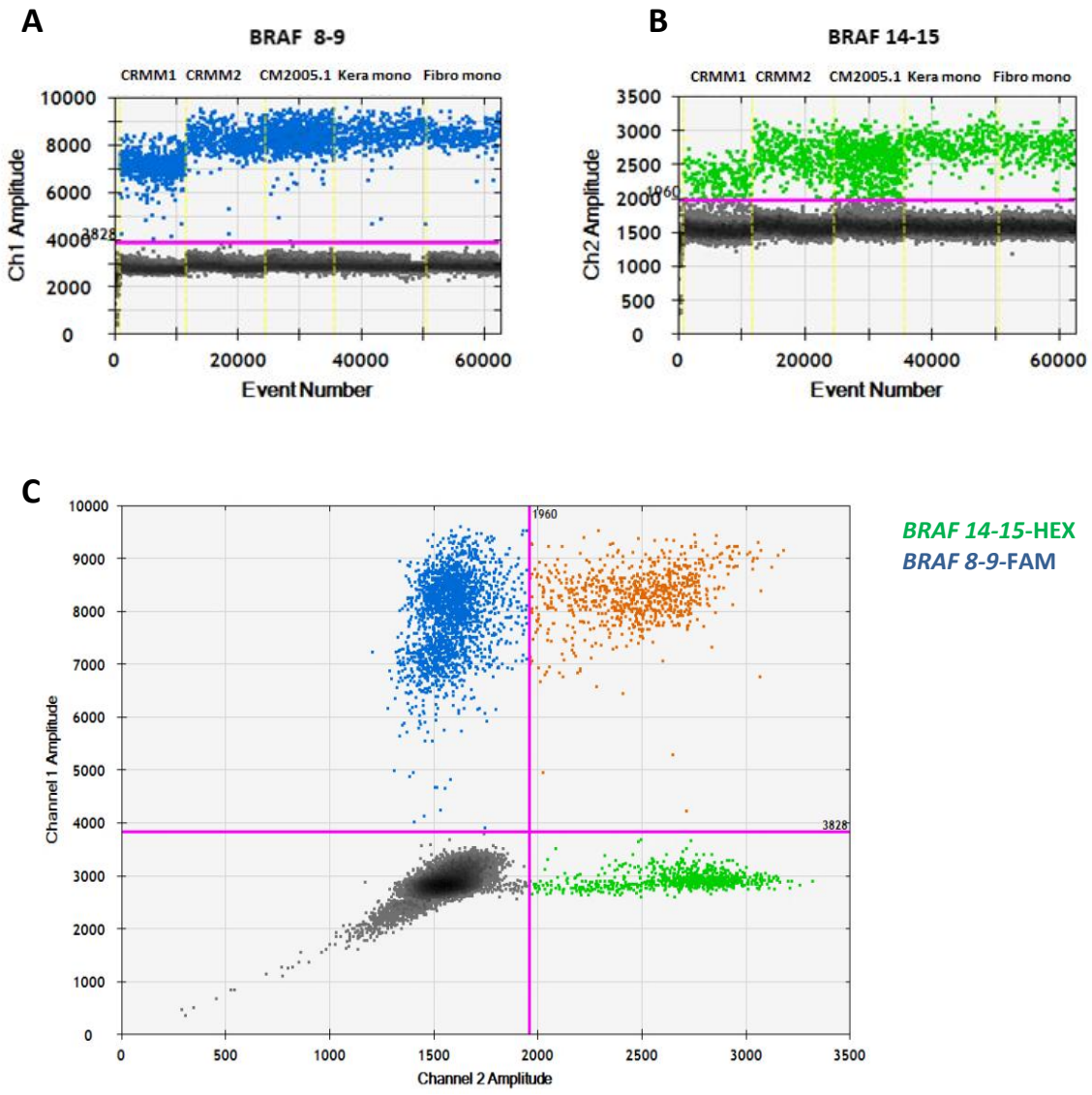

Figure 11. One-dimensional plot representing positive and negative droplets of FAM-labelled *BRAF* 8-9 (A) and HEX-labelled *BRAF* 14-15 (B). In addition, the corresponding two-dimensional plot (C) is represented to visualize the different populations of droplets which have been formed after amplification.

The quantification of droplets containing *BRAF* 8-9 or *BRAF* 14-15 in all conjunctival melanoma cell lines and controls resulted in more droplets with *BRAF* 8-9 compared to droplets with *BRAF* 14-15 (Figure 12).

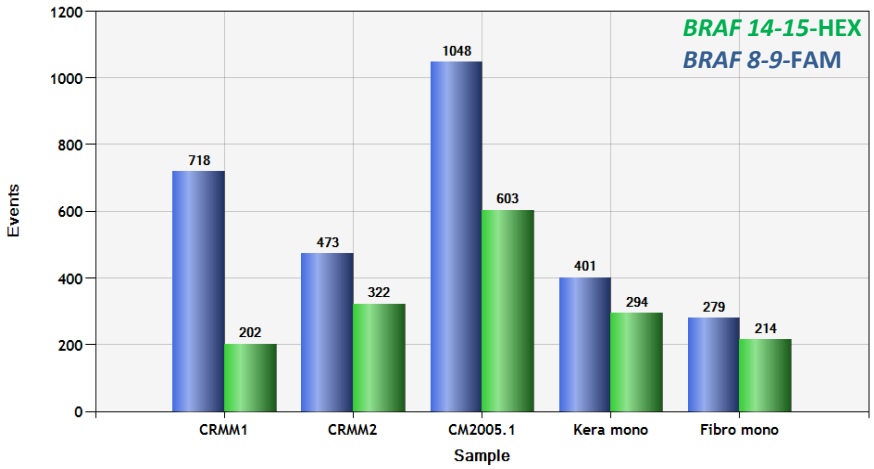

Figure 12. Event graph representing the quantity of positive droplets containing *BRAF* 8-9 or *BRAF* 14-15 in different cDNA conjunctival melanoma cell lines, keratinocytes and fibroblasts.

The initial target concentrations of *BRAF 8-9* and *BRAF 14-15*, appeared to be the lowest in CRMM2 compared to CRMM1 and CM2005.1 (Figure 13). In addition, a higher concentration of *BRAF* 8-9 was detected when compared to *BRAF* 14-15 in all samples, including controls. ddPCR revealed the ratios between *BRAF* 8-9 and *BRAF* 14-15 initial sample concentrations which showed a high variety from each other.

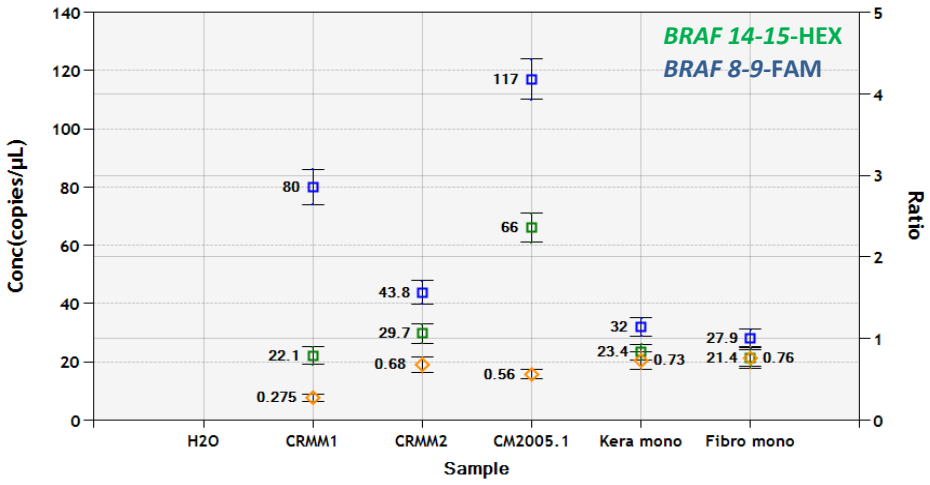

Figure 13. Initial target concentrations of *BRAF* 8-9 and *BRAF* 14-15 in different cDNA conjunctival melanoma cell lines plotted in copies/ µL with its corresponding ratios. Sample concentrations were corrected with Poisson's law.

Testing 'BRAF 8-9*' and 'BRAF* qp 14-15*' primers with ddPCR*

ddPCR using a non-*BRAF* V600(E) overlapping qp 14-15 reverse primer resulted in a separation between positive and negative droplets. All samples showed *BRAF* 8-9 (Figure 14A) and *BRAF* 14-15 (Figure 14B) positive droplets, including keratinocytes, fibroblasts and normal skin samples which were used as controls. Some positive droplets contained both *BRAF* 8-9 and *BRAF* 14-15 (Figure 14C).

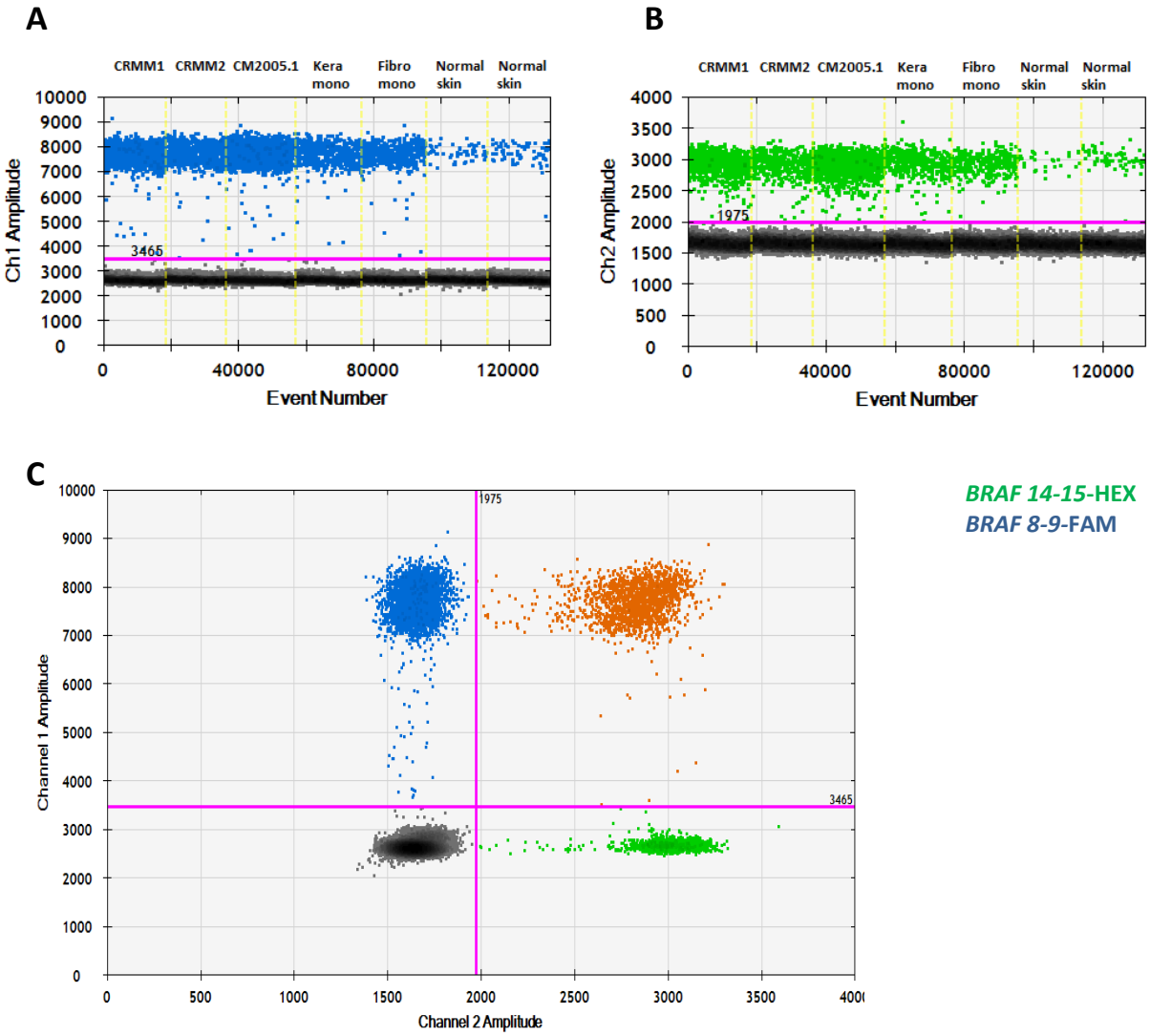

Figure 14. One-dimensional plot representing positive and negative droplets of FAM-labelled *BRAF* 8-9 (A) and HEX-labelled *BRAF* 14-15 (B). In addition, the corresponding two-dimensional plot (C) is represented to visualize the different populations of droplets which have been formed after amplification.

The quantification of droplets containing *BRAF* 8-9 or *BRAF* 14-15 in all conjunctival melanoma cell lines and controls resulted in more droplets with *BRAF* 8-9 compared to droplets with *BRAF* 14-15 (Figure 15).

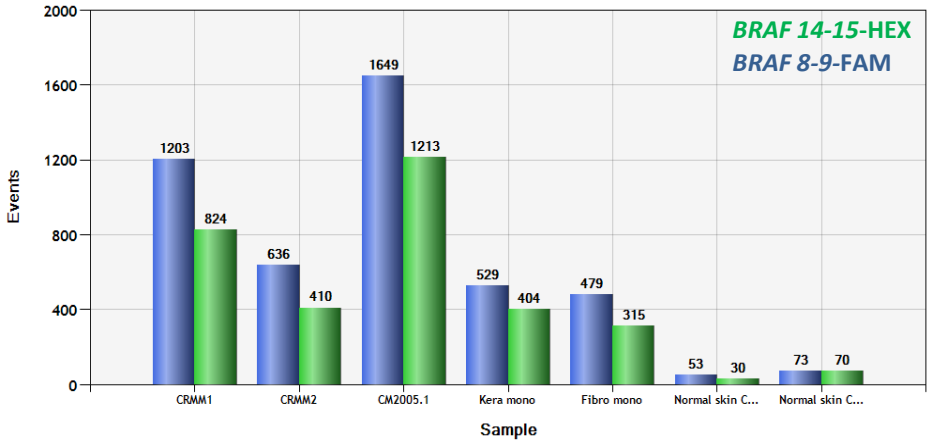

Figure 15. Event graph representing the quantity of positive droplets containing *BRAF* 8-9 or *BRAF* 14-15 in different cDNA conjunctival melanoma cell lines, keratinocytes and fibroblasts and normal skin.

The initial target concentrations of *BRAF 8-9* and *BRAF 14-15* has shown to be the lowest in CRMM2 compared to CRMM1 and CM2005.1 (Figure 16). In addition, a higher concentration of *BRAF* 8-9 was detected when compared to *BRAF* 14-15 in all samples, including controls. Moreover, ratios between *BRAF 8-9* and *BRAF 14-15* concentrations showed stable values compared to each other.

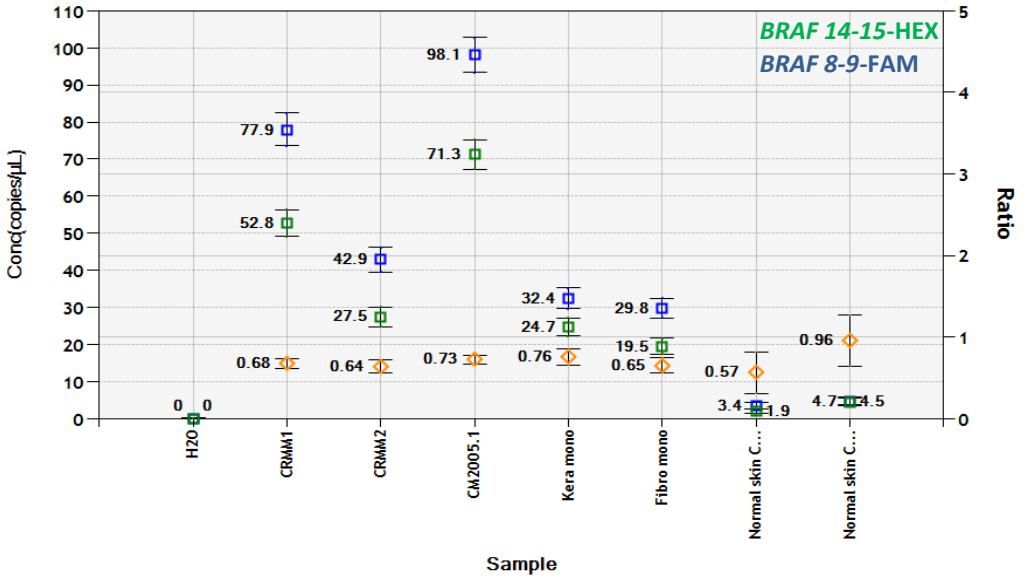

Figure 16. Initial target concentrations of *BRAF* 8-9 and *BRAF* 14-15 in different cDNA conjunctival melanoma cell lines plotted in copies/ µL with its corresponding ratios. Sample concentrations were corrected with Poisson's law.

4.2 Quantification of tumor-infiltrating T cells

After amplification of target DNA (*TTC5* or ΔD) with ddPCR, positive *TTC5* and ΔD droplets and negative droplets were counted in order to quantify the T cells. The threshold separated positive droplets (containing amplified ΔD and/or *TTC5*) and negative droplets (droplets without amplified target DNA). NA tissue samples showed HEX-labelled *TTC5* (Figure 17A) and FAM-labelled ΔD (Figure 17B) positive droplets. Nevertheless, no clear separation between positive and negative droplets could be made since intermediate droplets were shown in both *TTC5* and ΔD droplets. Less positive droplets were detected once a higher dilution factor was used. Droplets were divided in four droplet populations: HEX-/FAM- droplets which contained no target (black), HEX+/FAM- droplets which contained only *TTC5* (green), HEX-/FAM+ which contained only ΔD (blue) and HEX+/FAM+ which contained both *TTC5* and ΔD (orange) (Figure 17C).

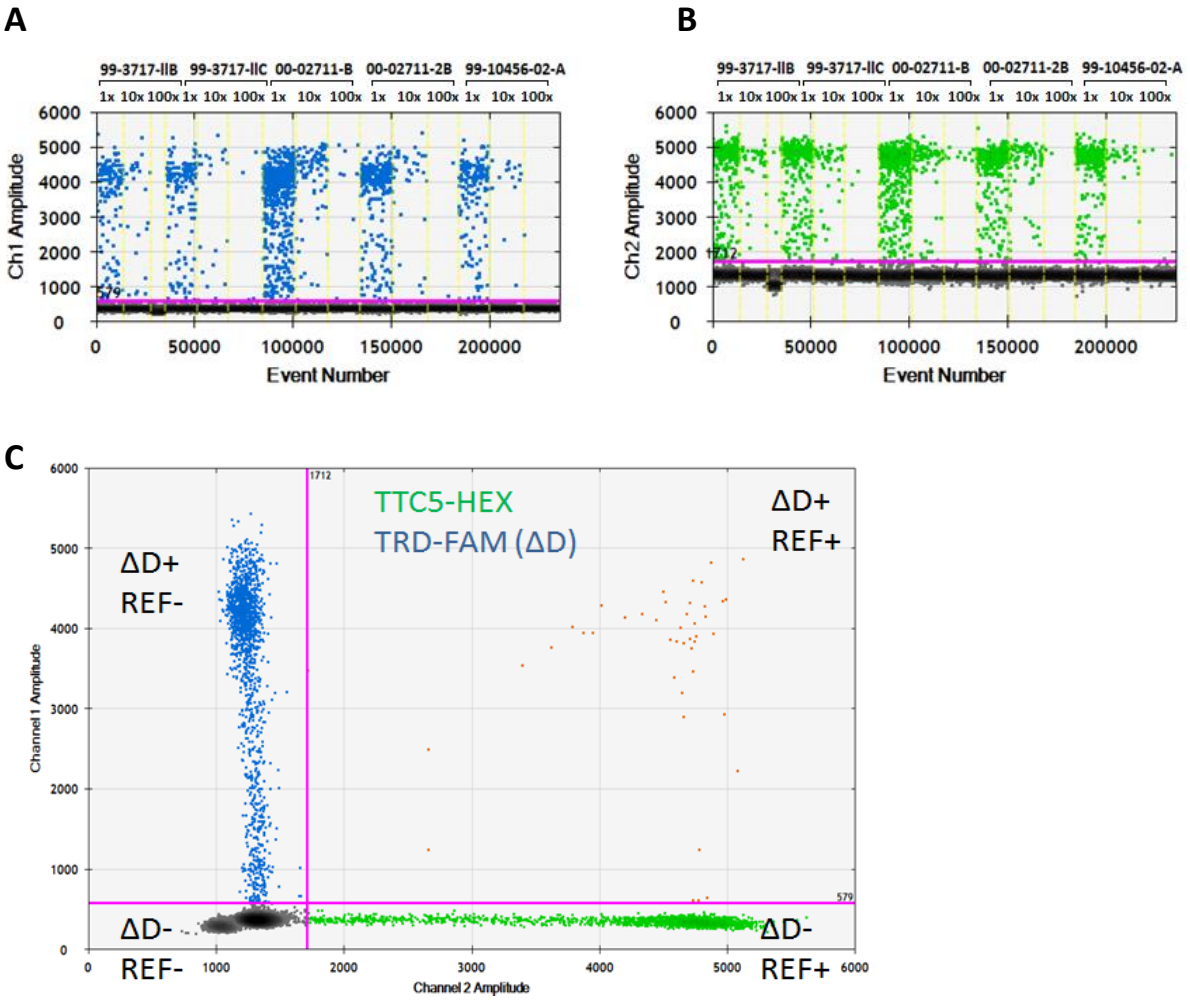

Figure 17. One-dimensional plot representing positive and negative droplets of FAM-labelled ΔD (A) and HEX-labelled *TTC5* (B). In addition, the corresponding two-dimensional plot is represented to visualize the different populations of droplets which have been formed after amplification.

The quantification of droplets containing ΔD or reference gene *TTC5* in all NA tissue samples resulted frequently in more droplets with *TTC5* compared to droplets with ΔD, though 10x diluted NA sample 00-027-11-B shows more ΔD positive droplets than *TTC5* positive droplets (Figure 18).

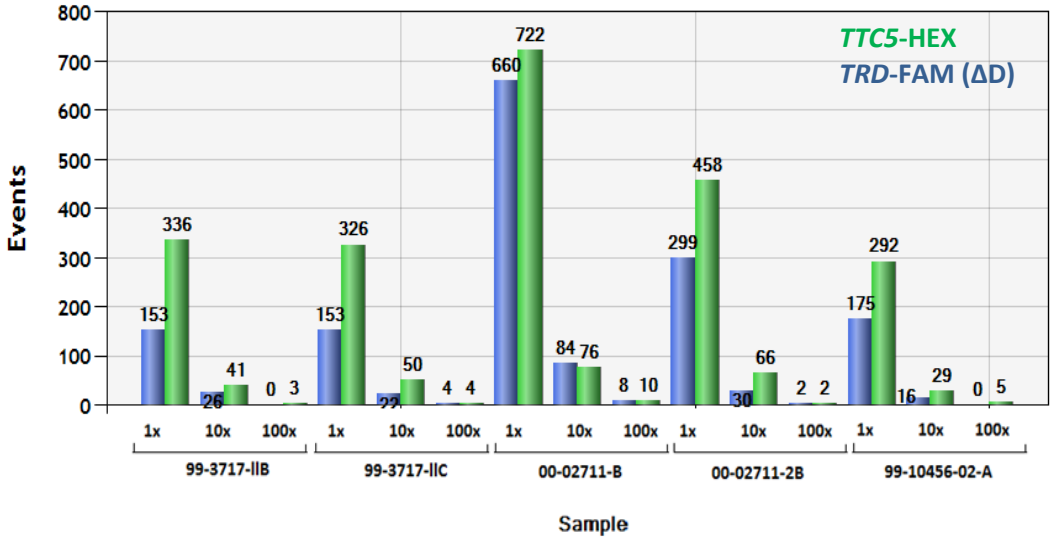

Figure 18. Event graph representing positive droplets containing ΔD or reference gene *TTC5* in different FFPE tissue samples.

Quantified positive droplets, corrected by Poisson's law resulted the initial target concentrations of *TTC5* and ΔD and the corresponding ratios between them (Figure 19). The concentration decreased once the sample is diluted, however a bigger error bar was observed.

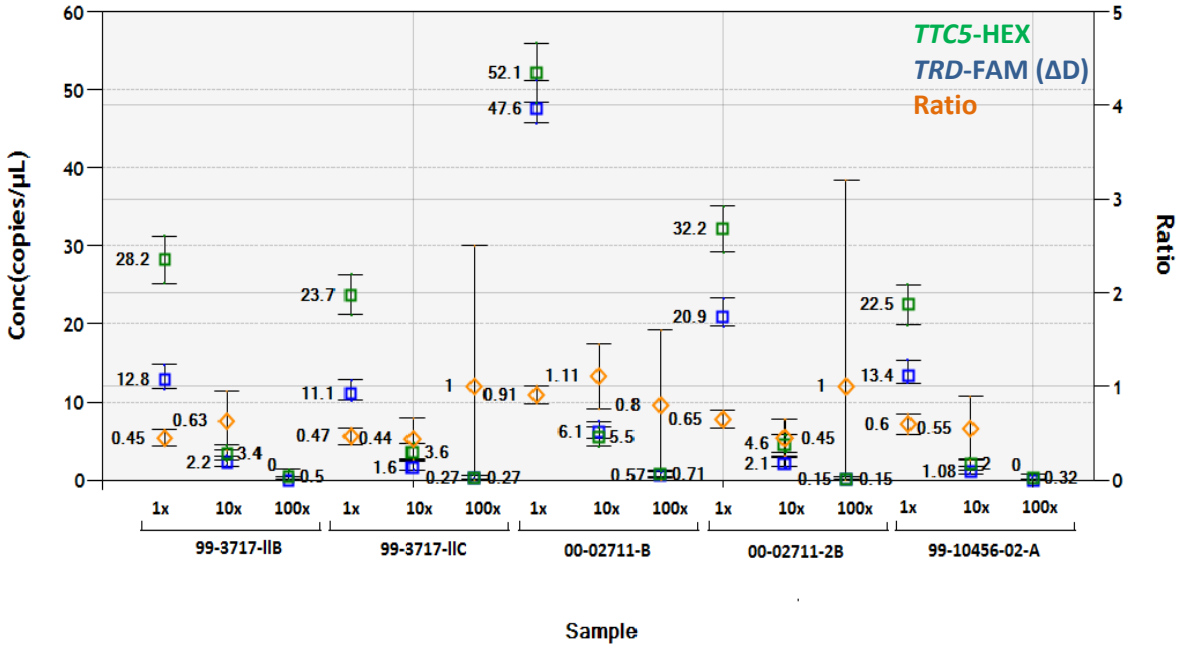

Figure 19. Initial target concentrations of *TTC5* and ΔD in FFPE tissue samples plotted in copies/ µL with its corresponding ratios. Sample concentrations were corrected with Poisson's law.

The T cell fractions showed that sample 99-3717-IIB and 99-3717-IIC, which originated from the same surgical excision, contain almost the same fraction of T cells, respectively 55% and 53% (Figure 20). However, samples 00-02711-B and 00-02711-2B show a difference in T cell fractions, respectively 9% and 35%. Sample 99-10456-02-A has a T cell fraction of 40%. Additional corresponding raw data is shown in table S4 in appendix 2.

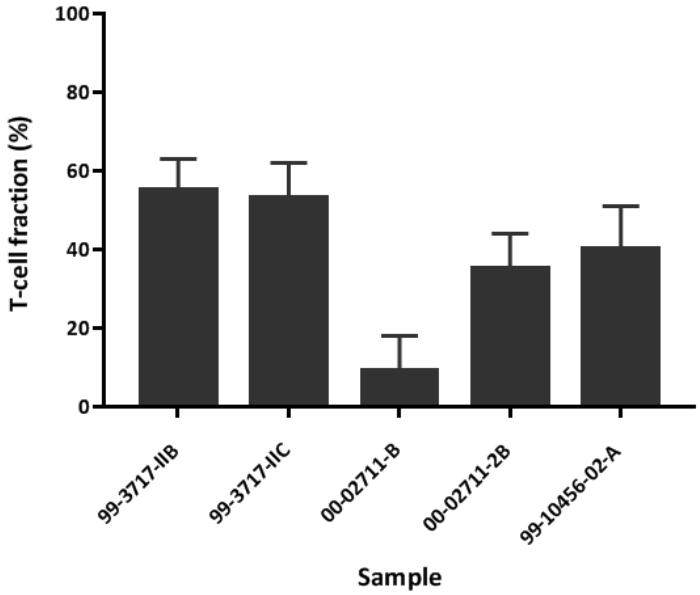

Figure 20. Calculated T cell fractions expressed in percentages in different FFPE tissue samples.

5. Interpretation and conclusion

Amplification of *BRAF* 8-9 and *BRAF* 14-15 by qPCR, allowed us to measure the relative normalized gene expression levels in cDNA of conjunctival melanoma cell lines. Based on relative normalized expressions and cq values found, it was observed that expression levels of *BRAF* 8-9 and *BRAF* 14-15 were not the same within the samples. This was the case when using *BRAF* 8-9 primer sets and a forward *BRAF* 14-15 primer combined with a *BRAF* qp 14-15 reverse primer. However when using *BRAF* 14-15 primer sets, equal *BRAF* 14-15 expressions were observed in all cell lines. Dissociation-characteristics of amplified target cDNA occurred equally during heating before 80ºC in each sample, meaning that no primer-dimers were formed and that no non-specific products were amplified. Altogether, based on different expression levels between exons *BRAF* 8-9 and *BRAF* 14-15, it can be asserted that splice variants were present.

The ddPCR assay showed an increased *BRAF* 8-9 expression compared to *BRAF* 14-15 expression in all conjunctiva melanoma cell lines and controls. Again a difference between expression levels was found. This finding was in concordance with the qPCR assay. However, analysis of the initial concentrations showed that the ratios between *BRAF* 8-9 and *BRAF* 14-15 were not equivalent. Moreover, positive droplets with *BRAF* 14-15 in CRMM1 and CM2005.1 showed abundant intermediate droplets that fell between the major positive and negative bands. This was an indication that the amplification of *BRAF* 14-15 might have gone wrong. One of the reasons for this observation might be that splice variants were present. Nevertheless, it was known that CRMM2 did not harbor the *BRAF* V600E mutation. Indeed, no intermediate droplets were observed. On the contrary, it was also known that CRMM1 and CM2005.1 harbored the *BRAF* V600E mutation. This fact indicated that the genetic sequence was different and that primer annealing might not have worked properly. The *BRAF* 14-15 reverse primer spanned the *BRAF* V600E mutation and consequently caused the formation of intermediate droplets. The reverse *BRAF* 14-15 primer was therefore the cause of inappropriate amplification in both ddPCR and qPCR.

Since the *BRAF* 14-15 reverse primer was not suitable for amplification in all cell lines, it was decided to continue with the non-V600E-overlapping *BRAF* qp 14-15 reverse primer. This primer was subjected to a second ddPCR assay in combination with the previous used *BRAF* 14-15 forward primer. In all conjunctiva melanoma cell lines and controls, comparable gene expression patterns between *BRAF* 8-9 and *BRAF* 14-15 were observed. In addition, *BRAF* 8-9 expression was higher compared to *BRAF* 14-15 expression. These findings were in accordance with the previous ddPCR assay. Yet, determination of the ratio between *BRAF* 8-9 and *BRAF* 14-15 revealed some new insights: The ratio between *BRAF* 8-9 and *BRAF* 14-15 concentrations showed relatively stable values meaning that the expression patterns between the samples were the same. This finding was probably the consequence of using a primer that did not overlap the *BRAF* V600E mutation.

Genetic dissimilarity between T cells and non-T cells was exploited in dysplastic nevi and melanoma lesions for accurate quantification of T cells. Amplification of ΔD and *TTC5* resulted in more *TTC5* positive droplets compared to ΔD positive droplets in undiluted samples. This outcome was expected since it was known that all cells, including T cells expressed TTC5 biallelically in contrast to ΔD which was only expressed in non-T cells. Nevertheless, intermediate droplets were observed. This was caused due to the FFPE material as the DNA probably suffered from degradation due to the fixation process. In addition, it was observed that the dilution factor was not always in proportion to the

amount of positive droplets and concentrations found. Moreover, 10 times diluted sample 00-02711-B showed a ratio of 1.11. This would mean that a higher concentration of ΔD was present than *TTC5*. A possible explanation for these observations might be that *TTC5* signal was influenced by RNA interference during amplification of DNA all through the PCR reaction. Regarding to diluted samples, higher error bars were observed and therefore excluded from further analysis. When taking undiluted samples into account, it was observed that samples 99-3717-IIB and 99-3717-IIC, which were classified as melanoma, contained more T cells compared to samples 00-02711-B, 00-02711-2B and 99-10456-02-A, which were classified as dysplastic nevi. The difference in T cell fraction in dysplastic nevi 00-02711-B and 00-02711-2B, could be the consequence of the way of how sectioning of the tissue samples was performed after surgical excision.

In this project, the main objective was to optimize the quantification of molecular genetic changes by ddPCR technology. Our main research question was: In which quantities are *BRAF* splice variants and T cells present in the different progression stages of cutaneous melanoma and is the *BRAF* V600E mutation connected to the occurrence of splice variants? From the results, it can be concluded that **spice variants were present in the *BRAF* transcripts** since the *BRAF* 8-9 and *BRAF* 14-15 expression was not equal to each other. With regards to optimization of *BRAF* splice variant experiments, only **a combination of *BRAF* 14-15 forward primers and *BRAF* qp 14-15 reverse primers lead to a proper amplification of target exon *BRAF* 14-15 in both mutated and non-mutated cell lines.** Regarding to T cell quantification, it can be concluded that **melanoma contained more T cells than dysplastic nevi.** These findings are in accordance with our presuppositions. Yet, no conformation can be made on the exact genomic region where splice variants occurred, neither in conjunctival melanoma cell lines nor in NA of FFPE material. In addition, the exact connection to the *BRAF* V600E mutation remains unknown since the experiments require further optimization.

6. Discussion and future directions

Herein, it was described how the detection and quantification of *BRAF* splice variants and T cells was optimized using qPCR and/ or ddPCR. Exploiting genetic properties and dissimilarities in combination with primer- and probe design has revealed more insights in how molecular genetic changes could be quantified efficiently. Based on experiments performed on conjunctiva melanoma cell lines and FFPE material, generic ddPCR assays have shown to provide a relatively fast and sensitive way for quantifying genetic regions.

In contrast to ddPCR, qPCR has no digital dimension. However, it was initially a fast and cheaper method to exploit splice variants of the *BRAF* gene transcript in conjunctival melanoma cell lines. Our data demonstrated splice variant characteristics which is in accordance with multiple studies. Though, these studies often use resistant melanomas as a sample instead of conjunctival melanoma cell lines. It has recently been indicated that the *BRAF* transcript is commonly subjected to alternative splicing (Salton *et al*., 2015). Though, alternative splicing is a mechanism which often becomes activated as resistance mechanism against dabrafenib and vemurafenib (Poulikakos *et al*., 2011; Rizos *et al*., 2014). Two of our cell lines harbored the *BRAF* V600E mutation, however none of these cell lines were treated with dabrafenib and vemurafenib or any other therapeutic agent. Therefore, the absence of these chemical compounds might probably not always be associated with the appearance of *BRAF* splice variants. Opportunities for further optimization would be to threat *BRAF* V600E mutated cell lines with dabrafenib and vemurafenib to check the further effects on *BRAF* splice variants. A final step would be to implement this experimental set-up into a ddPCR experimental approach to quantify splice variants precisely. In addition, the examined transcripts, focused on exons *BRAF* 8-9 and *BRAF* 14-15, might be extended to a larger range to examine whether splicing also occurs in other regions of the *BRAF* gene. Further research in the *BRAF* 14-15 transcript might help to identify whether there is a connection with the *BRAF* V600E mutation.

Measuring the most deleted sequence in the rearranging TCR gene ΔD allowed us to measure T cell fractions in FFPE material by duplex ddPCR. T cell proportions in body fluids or solid tissue are commonly quantified using flow cytometry and immunohistochemistry. Nevertheless, these techniques require advanced standardization and are dependent on sample type and quality of input material (Walker, 2006; Wood *et al*., 2013) Therefore, a recent study has developed ddPCR assays which provide a sensitive way for accurate quantification of T cells (Zoutman *et al*., 2017). Nevertheless, our experimental design using FFPE material requires still more optimization steps to enhance the experimental validity and accuracy of our results. NA isolation from FFPE material can probably be further improved. In addition, it might be the case that TTC5 signal was interfered by RNA. Therefore, further research should be performed to test this by performing for example extra purification steps.

Although, we could not present an accurate occurrence of *BRAF* splice variants, the method used to perform accurate quantification of different genomic regions showed to be promising for further research. In contrast to qPCR used in the past, ddPCR does not only detect the mutations with high specificity but also makes it possible to quantify the T cell fractions in cutaneous melanoma samples. We believe that using this technology, together with incorporating more melanoma-related samples from different progression stages, will contribute to a better discrimination between benign and

malignant melanoma. Moreover, a better understanding of cutaneous melanoma development can lead to new biomarkers for early diagnosis and/or improved targeted therapies.

7. Acknowledgements

The author wants to thank the Dermatology and the Ophthalmology department at the Leiden University Medical Central, Leiden, The Netherlands for their contribution to this project. In particular, my gratitude goes to Nelleke Gruis, Pieter van der Velden, Mieke Versluis, Mijke Visser, Wim Zoutman and Rogier Nell for their supervision, stimulating discussions and overall contribution in this project. Also to Coby Out for the technical assistance and Nicole Kukutsch for reviewing the tissue samples to confirm the clinical diagnosis.

Bibliography

Balch, C. M., Gershenwald, J. E., Soong, S. J., Thompson, J. F., Atkins, M. B., Byrd, D. R., . . . Sondak, V. K. (2009). Final version of 2009 AJCC melanoma staging and classification. *J Clin Oncol, 27*(36), 6199-6206. doi: 10.1200/JCO.2009.23.4799

Balch, C. M., Soong, S. J., Atkins, M. B., Buzaid, A. C., Cascinelli, N., Coit, D. G., . . . Thompson, J. F. (2004). An evidence-based staging system for cutaneous melanoma. *CA Cancer J Clin, 54*(3), 131-149; quiz 182-134.

Bandarchi, B., Ma, L., Navab, R., Seth, A., & Rasty, G. (2010). From melanocyte to metastatic malignant melanoma. *Dermatol Res Pract, 2010*. doi: 10.1155/2010/583748

Bastian, B. C. (2014). The molecular pathology of melanoma: an integrated taxonomy of melanocytic neoplasia. *Annu Rev Pathol, 9*, 239-271. doi: 10.1146/annurev-pathol-012513-104658

Black, D. L. (2003). Mechanisms of alternative pre-messenger RNA splicing. *Annu Rev Biochem, 72*, 291-336. doi: 10.1146/annurev.biochem.72.121801.161720

Bruno, W., Martinuzzi, C., Andreotti, V., Pastorino, L., Spagnolo, F., Dalmasso, B., . . . Italian Melanoma, I. (2017). Heterogeneity and frequency of BRAF mutations in primary melanoma: Comparison between molecular methods and immunohistochemistry. *Oncotarget, 8*(5), 8069-8082. doi: 10.18632/oncotarget.14094

Chapman, P. B., Hauschild, A., Robert, C., Haanen, J. B., Ascierto, P., Larkin, J., . . . Group, B.-S. (2011). Improved survival with vemurafenib in melanoma with BRAF V600E mutation. *N Engl J Med, 364*(26), 2507-2516. doi: 10.1056/NEJMoa1103782

Charles A Janeway, J., Paul Travers, Mark Walport, and Mark J Shlomchik. (2001). *Immunobiology* (5 ed.): New York: Garland Science.

Chen, C. F., Ruiz-Vega, R., Vasudeva, P., Espitia, F., Krasieva, T. B., de Feraudy, S., . . . Ganesan, A. K. (2017). ATR Mutations Promote the Growth of Melanoma Tumors by Modulating the Immune Microenvironment. *Cell Rep, 18*(10), 2331-2342. doi: 10.1016/j.celrep.2017.02.040

Dik, W. A., Pike-Overzet, K., Weerkamp, F., de Ridder, D., de Haas, E. F., Baert, M. R., . . . Staal, F. J. (2005). New insights on human T cell development by quantitative T cell receptor gene rearrangement studies and gene expression profiling. *J Exp Med, 201*(11), 1715-1723. doi: 10.1084/jem.20042524

Elder, D. E. (2016). Melanoma progression. *Pathology, 48*(2), 147-154. doi: 10.1016/j.pathol.2015.12.002

Fridman, W. H., Galon, J., Pages, F., Tartour, E., Sautes-Fridman, C., & Kroemer, G. (2011). Prognostic and predictive impact of intra- and peritumoral immune infiltrates. *Cancer Res, 71*(17), 5601-5605. doi: 10.1158/0008-5472.CAN-11-1316

Gajewski, T. F., Meng, Y., & Harlin, H. (2006). Immune suppression in the tumor microenvironment. *J Immunother, 29*(3), 233-240. doi: 10.1097/01.cji.0000199193.29048.56

Hodges, E., Krishna, M. T., Pickard, C., & Smith, J. L. (2003). Diagnostic role of tests for T cell receptor (TCR) genes. *J Clin Pathol, 56*(1), 1-11.

Hodis, E., Watson, I. R., Kryukov, G. V., Arold, S. T., Imielinski, M., Theurillat, J. P., . . . Chin, L. (2012). A landscape of driver mutations in melanoma. *Cell, 150*(2), 251-263. doi: 10.1016/j.cell.2012.06.024

Holderfield, M., Deuker, M. M., McCormick, F., & McMahon, M. (2014). Targeting RAF kinases for cancer therapy: BRAF-mutated melanoma and beyond. *Nat Rev Cancer, 14*(7), 455-467. doi: 10.1038/nrc3760

Houghton, A. N., Gold, J. S., & Blachere, N. E. (2001). Immunity against cancer: lessons learned from melanoma. *Curr Opin Immunol, 13*(2), 134-140.

Hussain, M. R., Baig, M., Mohamoud, H. S., Ulhaq, Z., Hoessli, D. C., Khogeer, G. S., . . . Al-Aama, J. Y. (2015). BRAF gene: From human cancers to developmental syndromes. *Saudi J Biol Sci, 22*(4), 359-373. doi: 10.1016/j.sjbs.2014.10.002

Keijser, S., Maat, W., Missotten, G. S., & de Keizer, R. J. (2007). A new cell line from a recurrent conjunctival melanoma. *Br J Ophthalmol, 91*(11), 1566-1567. doi: 10.1136/bjo.2006.110841

Key Statistics for Melanoma Skin Cancer. (2017). from https://www.cancer.org/cancer/melanoma-skin-cancer/about/key-statistics.html

Krauthammer, M., Kong, Y., Ha, B. H., Evans, P., Bacchiocchi, A., McCusker, J. P., . . . Halaban, R. (2012). Exome sequencing identifies recurrent somatic RAC1 mutations in melanoma. *Nat Genet, 44*(9), 1006-1014. doi: 10.1038/ng.2359

Li, B., Li, T., Pignon, J. C., Wang, B., Wang, J., Shukla, S. A., . . . Liu, X. S. (2016). Landscape of tumor-infiltrating T cell repertoire of human cancers. *Nat Genet, 48*(7), 725-732. doi: 10.1038/ng.3581

Martin TA, Y. L., Sanders AJ, *et al*. (2013). Cancer Invasion and Metastasis: Molecular and Cellular Perspective. . *Landes Bioscience*.

McCain, J. (2013). The MAPK (ERK) Pathway: Investigational Combinations for the Treatment Of BRAF-Mutated Metastatic Melanoma. *P T, 38*(2), 96-108.

Mihajlovic, M., Vlajkovic, S., Jovanovic, P., & Stefanovic, V. (2012). Primary mucosal melanomas: a comprehensive review. *Int J Clin Exp Pathol, 5*(8), 739-753.

Miller, A. J., & Mihm, M. C., Jr. (2006). Melanoma. *N Engl J Med, 355*(1), 51-65. doi: 10.1056/NEJMra052166

Nareyeck, G., Wuestemeyer, H., von der Haar, D., & Anastassiou, G. (2005). Establishment of two cell lines derived from conjunctival melanomas. *Exp Eye Res, 81*(3), 361-362. doi: 10.1016/j.exer.2005.04.018

National Cancer Institute. (2017) (pp. MEK: A Single Drug Target Shows Promise in Multiple Cancers): National Cancer Institute.

National Center for Biotechnology Information. (2017). 2017, from https://www.ncbi.nlm.nih.gov/gene/673

Poulikakos, P. I., Persaud, Y., Janakiraman, M., Kong, X., Ng, C., Moriceau, G., . . . Solit, D. B. (2011). RAF inhibitor resistance is mediated by dimerization of aberrantly spliced BRAF(V600E). *Nature, 480*(7377), 387-390. doi: 10.1038/nature10662

Rizos, H., Menzies, A. M., Pupo, G. M., Carlino, M. S., Fung, C., Hyman, J., . . . Long, G. V. (2014). BRAF inhibitor resistance mechanisms in metastatic melanoma: spectrum and clinical impact. *Clin Cancer Res, 20*(7), 1965-1977. doi: 10.1158/1078-0432.CCR-13-3122

Salton, M., Kasprzak, W. K., Voss, T., Shapiro, B. A., Poulikakos, P. I., & Misteli, T. (2015). Inhibition of vemurafenib-resistant melanoma by interference with pre-mRNA splicing. *Nat Commun, 6*, 7103. doi: 10.1038/ncomms8103

Shain, A. H., Yeh, I., Kovalyshyn, I., Sriharan, A., Talevich, E., Gagnon, A., . . . Bastian, B. C. (2015). The Genetic Evolution of Melanoma from Precursor Lesions. *N Engl J Med, 373*(20), 1926-1936. doi: 10.1056/NEJMoa1502583

Spagnolo, F., Ghiorzo, P., & Queirolo, P. (2014). Overcoming resistance to BRAF inhibition in BRAF-mutated metastatic melanoma. *Oncotarget, 5*(21), 10206-10221. doi: 10.18632/oncotarget.2602

Talmadge, J. E. (2011). Immune cell infiltration of primary and metastatic lesions: mechanisms and clinical impact. *Semin Cancer Biol, 21*(2), 131-138. doi: 10.1016/j.semcancer.2010.12.002

Vandesompele, J., De Preter, K., Pattyn, F., Poppe, B., Van Roy, N., De Paepe, A., & Speleman, F. (2002). Accurate normalization of real-time quantitative RT-PCR data by geometric averaging of multiple internal control genes. *Genome Biol, 3*(7), RESEARCH0034.

Volinsky, N., & Kholodenko, B. N. (2013). Complexity of receptor tyrosine kinase signal processing. *Cold Spring Harb Perspect Biol, 5*(8), a009043. doi: 10.1101/cshperspect.a009043

Walker, R. A. (2006). Quantification of immunohistochemistry--issues concerning methods, utility and semiquantitative assessment I. *Histopathology, 49*(4), 406-410. doi: 10.1111/j.1365-2559.2006.02514.x

Wood, B., Jevremovic, D., Bene, M. C., Yan, M., Jacobs, P., Litwin, V., & Group, I. I. W. (2013). Validation of cell-based fluorescence assays: practice guidelines from the ICSH and ICCS - part V - assay performance criteria. *Cytometry B Clin Cytom, 84*(5), 315-323. doi: 10.1002/cyto.b.21108

World Health Organization. (2017). from http://www.who.int/uv/faq/skincancer/en/index1.html

Zoutman, W. H., Nell, R. J., Versluis, M., van Steenderen, D., Lalai, R. N., Out-Luiting, J. J., . . . van der Velden, P. A. (2017). Accurate Quantification of T Cells by Measuring Loss of Germline T-Cell Receptor Loci with Generic Single Duplex Droplet Digital PCR Assays. *J Mol Diagn, 19*(2), 236-243. doi: 10.1016/j.jmoldx.2016.10.006

Appendix 1. Primer and probe information

Table S1. Primer information *BRAF* 8-9 and *BRAF* 14-15.

Primer name	Primer	Sequence	Genomic feature	Spans *BRAF* V600E?	length	Tm (C°)	GC (%)
BRAF 8-9 F	Forward primer (10 µ mol·L^{-1})	5'-GGCAACGAG-ACCGATCCTC-3'	Exon 8	No	19	67.2	63.1
BRAF 8-9 R	Reverse primer (10 µ mol·L^{-1})	5'-TCCTCCATCAC-CACGAAATCCT-3'	Exon 9	No	22	68.8	50.0
BRAF 14-15 F	Forward primer (10 µ mol·L^{-1})	5'-TGCACAGGGC-ATGGATTACTTA-3'	Exon 14	No	22	66.2	45.4
BRAF 15-15 R	Reverse primer (10 µ mol·L^{-1})	5'-CCCACTCCATC-GAGATTTCAC-3'	Exon 15	Yes	21	65.7	52.3
BRAF qp 14-15 R	Reverse primer (10 µ mol·L^{-1})	5'- GGGACCCACTC-CATCGAGATTTC -3'	Exon 15	No	23	NA	NA

Table S2. Probe information *BRAF* 8-9 and *BRAF* 14-15.

Probe	Sequence	Label	Genomic feature	length	Tm (C°)	GC (%)
BRAF 8-9 (10 µ mol·L^{-})	5'-TCAGCTCCCAAT-GTGCATATAAACA-3'	FAM	Exon 8-9	25	68.0	40.0
BRAF 14-15 (10 µ mol·L^{-})	5'-CGCCAAGTCAA-TCATCCACAGA-3'	HEX	Exon 14-15	22	69.4	50.0

Appendix 2. Additional experimental data

Table S3. Cycles of quantification demonstrated by qPCR for *BRAF* 14-15 and *BRAF* 8-9 in conjunctival melanoma cell lines using *BRAF* 8-9 primer set and *BRAF* 14-15 forward primer in combination with *BRAF* qp 14-15 reverse primer.

Fluorophore	Target	cDNA sample	Cq value	Cq value (AVG)
SYBR	*BRAF* 14-15	CRMM1	26.19 26.38	26.29
SYBR	*BRAF* 14-15	CRMM2	27.17 27.18	27.18
SYBR	*BRAF* 14-15	CM2005.1	26.02 25.84	25.93
SYBR	*BRAF* 8-9	CRMM1	25.60 26.74	26.17
SYBR	*BRAF* 8-9	CRMM2	26.53 27.45	26.99
SYBR	*BRAF* 8-9	CM2005.1	25,24 N.A.	25.24

Table S4. Calculated T cell fractions expressed in percentages in different FFPE tissue samples.

FFPE NA sample	Concentration target probe FAM (copies/uL)	Concentration Ref probe HEX (copies/uL)	T cell fraction (%)	+ Error (%)	- Error (%)
99-3717-IIB	12.8	28.2	55	8	9
99-3717-IIC	11.1	23.7	53	9	9
00-02711-B	47.6	52.1	9	9	10
00-02711-2B	20.9	32.2	35	9	9
99-10456-02-A	13.4	22.5	40	11	11

Appendix 3. Confirmation of clinical diagnosis

Table S5. Confirmation of clinical diagnosis. The table shows the clinical diagnosis of samples 00-2711, 99-10456 and 99-3717 after reviewing by a dermatologist for validation.

Tissue sample	Nevus subtype after reviewing
00-2711	dysplastic nevus
99-10456	dysplastic nevus
99-3717	melanoma